



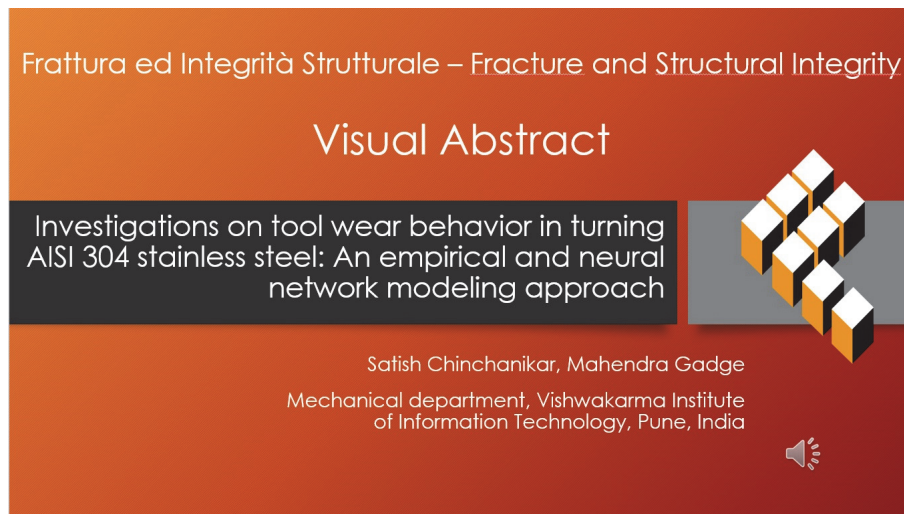
Investigations on tool wear behavior in turning AISI 304 stainless steel: An empirical and neural network modeling approach

Satish Chinchankar, Mahendra Gadge

Mechanical department, Vishwakarma Institute of Information Technology, Pune, India

satish.chinchankar@viit.ac.in, <http://orcid.org/0000-0002-4175-3098>

mahendra.gadge@viit.ac.in, <http://orcid.org/0000-0002-8603-8653>



Citation: Chinchankar, S., Gadge, M., Investigations on tool wear behavior in turning AISI 304 stainless steel: An empirical and neural network modeling approach, *Frattura ed Integrità Strutturale*, 67 (2024) 176-191.

Received: 06.09.2023

Accepted: 27.11.2023

Online first: 03.12.2023

Published: 01.01.2024

Copyright: © 2024 This is an open access article under the terms of the CC-BY 4.0, which permits unrestricted use, distribution, and reproduction in any medium, provided the original author and source are credited.

KEYWORDS. AISI 304, Tool wear, Fracture, Adhesion, Subtractive manufacturing, Modeling.

INTRODUCTION

Researchers are exploring the use of carbide tools for dry machining stainless steels to meet the increasing demand for cost-effective and environmentally friendly manufacturing processes. The cutting tool's performance is crucial, as the speed depends on the materials used. However, advancements in cemented carbide grades, coating deposition technologies, and materials have led to higher cutting parameters in the production of goods. These advancements have significantly improved the efficiency and productivity of the machining process, allowing manufacturers to meet the increasing demand for stainless steel products. Additionally, the use of coated tools reduces the need for coolant, minimizing waste and environmental impact.

The evaluation of flank wear is crucial in sustainable manufacturing, as it impacts product quality, and replacing tools before their tool life significantly impacts the machining economy. Flank wear refers to the gradual wear and tear occurring on the cutting edge of a tool during machining operations. By monitoring and evaluating flank wear, manufacturers can ensure that

tools are replaced at the optimum times, maximizing their tool life, and minimizing production downtime. Additionally, accurate evaluation of flank wear allows for proactive maintenance planning, reducing the risk of sudden tool failure and potential damage to workpieces. Researchers have made significant efforts to understand and model tool wear progression and mechanisms in metal cutting, but most models focus on machining using PCBN or ceramic inserts [1, 2, 3].

Dureja [4] created models for tool wear using a CBN tool, observing that cutting speed and feed significantly impact flank wear. Chincharikar and Choudhury et al. [5] created a flank wear model using Taylor's exponent and constant for turning hardened steel using carbide tools. Mohamad et al. [6] discovered plastic deformation and abrasion as presiding wear mechanisms during hard turning. Regression and artificial neural network (ANN) models were developed by Palanisamy and Shanmugasundaram [7] to forecast surface roughness and tool wear.

The ANN model has been found to be a promising and effective technique for mathematically modeling complicated and nonlinear wear behavior. This technique takes inspiration from the biological nervous system and models a variety of complex, nonlinear, and intricate real-world interactions. ANN assists in precisely simulating the nonlinear characteristics of composite materials and calculates how different input parameters will affect the material's performance. A team of researchers found that the quality and amount of data used for training an ANN model affect how well it performs. In order to reduce time and train an ANN model efficiently, it is further noted that a considerable selection of parameters must be chosen [8, 9]. The ANN modeling aids in comprehending the physics of the process, which would enhance process performance by enabling better process control. AISI 304 austenitic steel was turned by Kulkarni et al. [10] using multi-layer AlTiN/TiAlN-coated carbide tools. Their research revealed that feed considerably influenced the cutting forces, and cutting speed greatly affected the cutting temperature. When turning SS 304, Sharma and Gupta [11] found improved performance with coated carbide tools compared to uncoated tools. It is reported that the tool wear significantly affected by the cutting speed and cutting time [12, 13].

A group of researchers assessed tool wear during machining of stainless steel using different cooling techniques and coated tools [14, 15, 16]. However, the greatest obstacle to the widespread use of carbide tools for the high-speed machining of stainless steel is tool wear, which has a negative impact on workpiece quality. Hence, the creation of a trustworthy flank wear growth model will be quite beneficial. Researchers have developed ANN models to predict machining performance, but no models have been developed to predict the flank wear growth of coated carbide tools while turning AISI 304 stainless steel.

This study assesses tool wear, its forms, and wear mechanisms of the MTCVD-TiCN/Al₂O₃ coated carbide tool while turning AISI 304 stainless steel. The empirical and ANN models are built to assess flank wear growth. The study aims to provide insights into the performance and durability of the selected tool. The empirical and ANN models will enable accurate predictions of flank wear growth, aiding in optimizing tool life and improving machining efficiency. The created model is calibrated and validated while rotating at various cutting settings that were employed in the model's construction. Experiments were designed to cover a broader range of operating conditions to ensure the model's accuracy and applicability in practical machining scenarios.

EXPERIMENTAL DESIGN

On a CNC lathe, dry-turning tests on AISI 304 stainless steel were performed (Fig. 1). Cutting tests were performed using the most popular and widely used MTCVD-TiCN/Al₂O₃ coated cemented carbide tool with a geometry known as CNMG 120408 (an 80° diamond shape with a 0.8 mm nose radius) according to ISO. The insert was securely fastened to a tool holder, PCBNR 2525K12, which resulted in the orthogonal rake angle of -6°, inclination angle of -6°, tool cutting edge angle of 75°, and tool lead angle of 15°. The material composition is shown in Tab. 1.

C	Si	Mn	P	S	Cr	Ni	N	Fe
0.033	0.88	1.98	0.037	0.013	18.37	8.82	0.11	Balance

Table 1: Chemical composition of AISI 304 stainless steel (in wt. %).

Fig. 2(a) shows the microstructure of AISI 304 stainless steel. Uniform austenitic grain structure with no carbide precipitation along grain boundaries can be seen. Fig. 2(b) shows the cut-section of a multi-layer MTCVD-TiCN/Al₂O₃ coated tool. The average coating thickness of 17.6 μm can be seen. The thicker MTCVD coating's inner TiCN layer adheres to the substrate and provides toughness at the cutting edge, and the uppermost Al₂O₃ layer acts as a thermal barrier that offers resistance toward crater wear. Moreover, better coating adhesion lowers microchipping, edge buildup, burr formation,

and depth-of-cut notching. Images captured by a digital microscope and a scanning electron microscope (SEM) are used to describe various tool wear shapes and wear mechanisms discovered for these inserts. The results of this study give the industrial community the knowledge they need to make decisions about tool replacement policies and to impose restrictions on the cutting conditions that may be used while machining such metals.

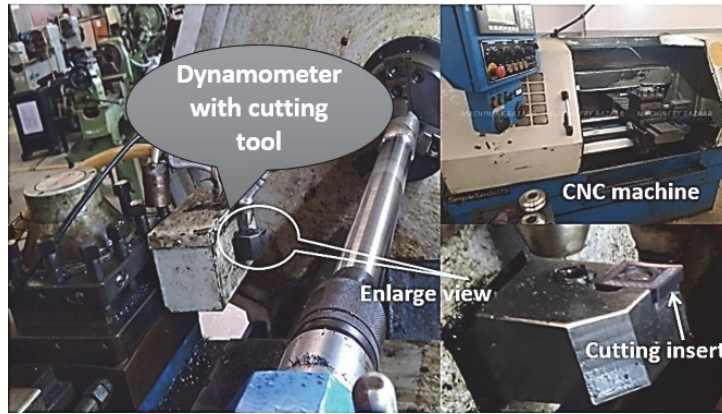


Figure 1: Experimental set-up.

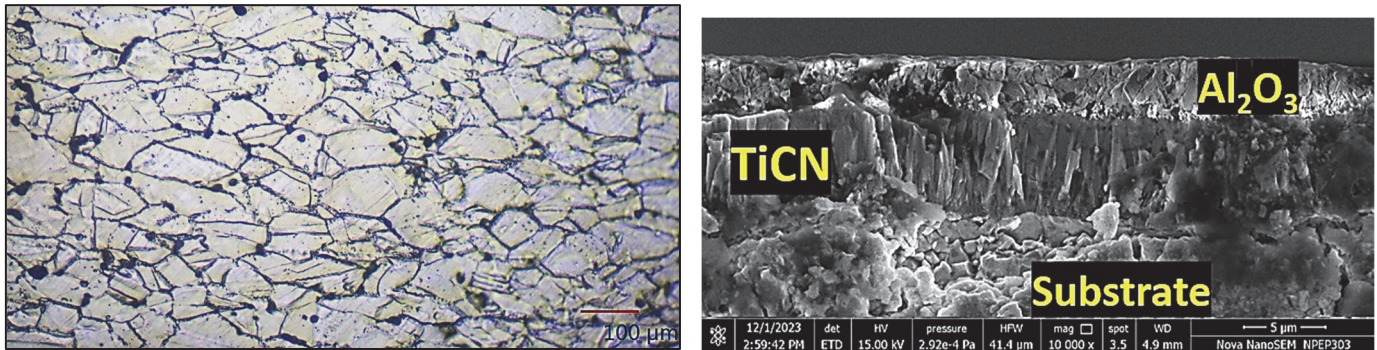


Figure 2: (a) Microstructure of AISI 304 stainless steel. (b) Cut-section of MTCVD-TiCN/Al₂O₃ coated tool.

Tab. 2 displays the cutting parameters utilized while turning AISI 304 stainless steel. Based on a review of the relevant literature, pilot experiments, and advice from the tool's maker, ranges for input variables were selected to ensure optimal cutting performance and minimum tool wear.

Expt. run														
R1	R2	R3	R4	R5	R6	R7	R8	R9	R10	R11	R12	R13	R14	R15
Cutting speed (V) (m/min)														
300	350	350	250	250	300	300	300	200	400	350	250	350	250	300
Feed (f) (mm/rev)														
0.1	0.08	0.12	0.08	0.12	0.05	0.1	0.15	0.1	0.1	0.08	0.12	0.12	0.08	0.1
Depth of cut (d) (mm)														
0.5	0.4	0.4	0.4	0.4	0.3	0.3	0.3	0.3	0.3	0.2	0.2	0.2	0.2	0.1

Table 2: Experimental matrix to assess the tool wear growth in turning AISI 304 stainless steel.

RESULTS AND DISCUSSION

In this section, the assessment of tool wear, its forms, and wear mechanisms are discussed. The study develops experimental-based mathematical and ANN models to obtain flank wear growth of MTCVD-TiCN/Al₂O₃ tools during turning AISI 304 stainless steel. The experimental-based mathematical model was developed by conducting cutting



tests under various cutting conditions and measuring flank wear growth. However, the ANN model was trained using the collected experimental data to predict flank wear growth based on input parameters.

Images captured by digital and scanning electron microscopes (SEM) are used to describe various tool wear shapes and wear mechanisms discovered for these inserts. The results of this study give the industrial community the knowledge they need to make decisions about tool replacement policies and to impose restrictions on the cutting conditions that may be used while machining such metals.

Flank wear growth for selected tool at experimental runs R1 to R15 as depicted in Tab. 2 is shown in Figs. 3 and 4. Plots demonstrate that the flank wear increases with cutting time and is primarily concentrated in three regions: the initial breakdown, the uniform wear rate, and the rapid cutting-edge breakdown. These three regions of wear on the flank face can be attributed to different mechanisms. The initial breakdown occurs due to the interaction between the cutting tool and the workpiece material, resulting in micro-chipping and minor fractures. The uniform wear rate region occurs when the tool has reached a stable state, where gradual abrasion and friction result in a consistent wear pattern. Finally, rapid cutting-edge breakdown is characterized by accelerated wear due to higher temperatures and increased forces during prolonged cutting operations.

Fig. 5 display insert images for different machining conditions, showing flank wear as predominant at lower speeds, followed by coating layer chipping and catastrophic failure at higher speeds. The insert images provide a clear visual representation of the effects of various cutting conditions on the tool. At lower speeds, flank wear is observed as the primary form of tool degradation, indicating gradual wear and tear on the cutting edge. As the speed increases, chipping of the coating layers becomes more prominent, suggesting that the coating is unable to withstand the higher forces and stresses involved. Finally, at higher speeds, catastrophic failure is evident, indicating complete tool breakdown and rendering it unusable for further machining operations.

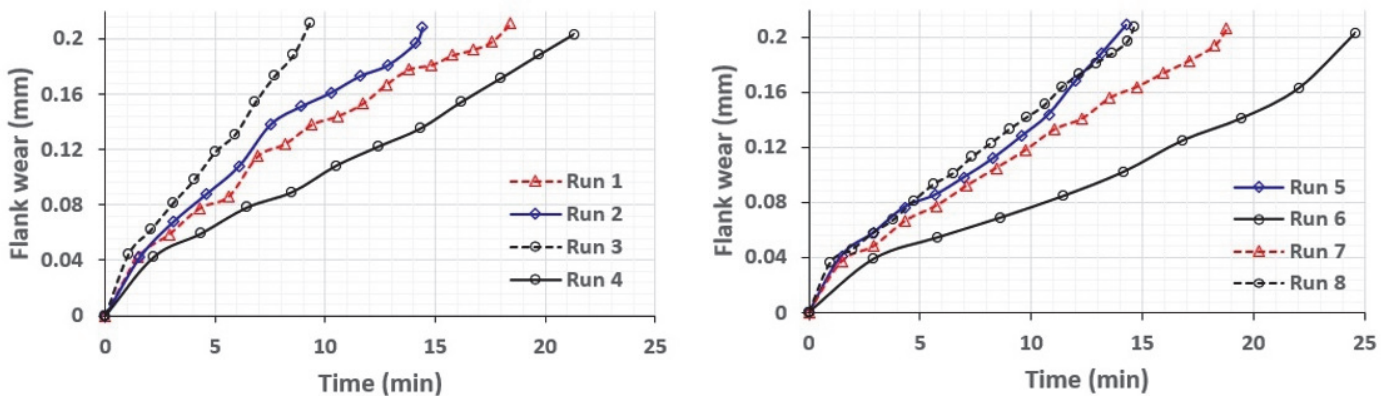


Figure 3: Flank wear when turning AISI 304 at run R1 to R8.

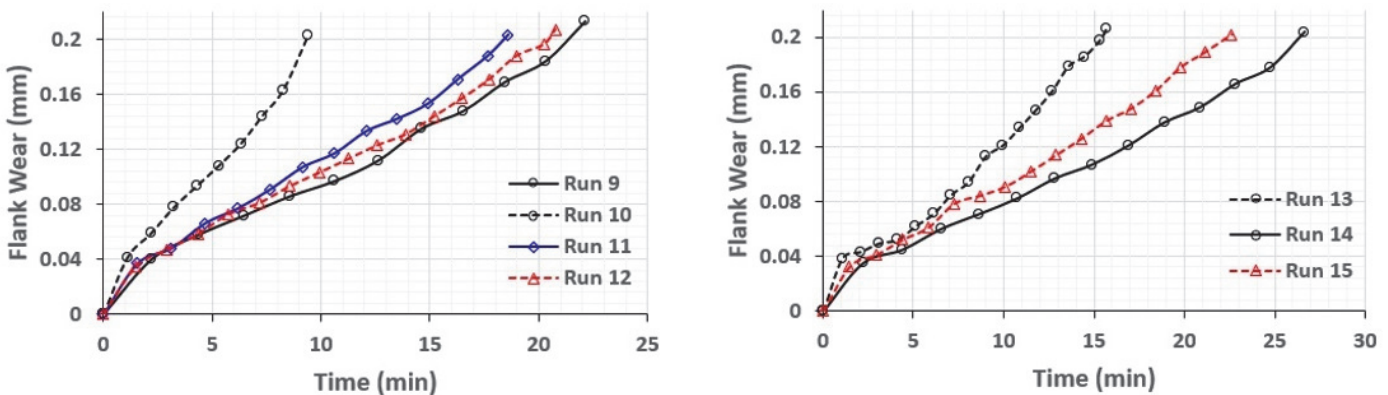


Figure 4: Flank wear when turning AISI 304 at run R9 to R15.

Higher tool life of 26.6 minutes can be seen as obtained for experimental run 14, i.e., at $V = 250$ m/min, $f = 0.08$ mm/rev, and $d = 0.2$ mm. Lower tool life of 9.3 minutes can be seen as obtained for experimental run 3, i.e., at $V = 350$ m/min, $f = 0.12$ mm/rev, and $d = 0.4$ mm. This tool failed because the coating layers peeled off due to the fast-moving chips breaking

the attached metal, causing an abrupt fracture. It is evident that reducing cutting parameters extends tool life. Regular tool inspections can help detect and address potential issues before they cause abrupt fractures by identifying signs of wear or damage.

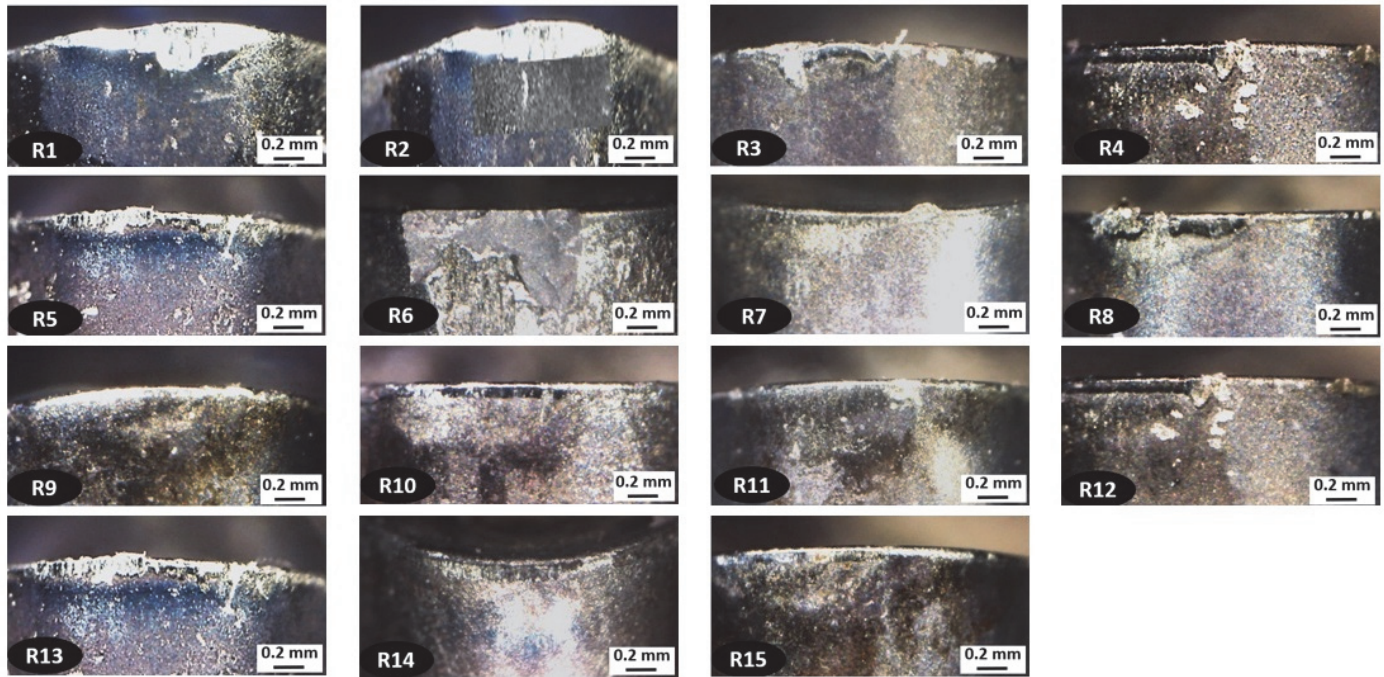


Figure 5: Flank wear when turning AISI 304 at run R1 to R15.

Tool wear forms and mechanisms

This section examines the tool wear forms and mechanisms of a selected tool while turning AISI 304 stainless steel using digital and SEM images. The main wear patterns identified were flank wear, coating chipping, and cutting-edge deformation. Figs. 6–10 show various wear patterns found on the tool after cutting. The tool is severely damaged by metal adhesion, coating delamination, chipping, and pitting. These issues greatly compromise the tool's performance and durability. Metal adhesion can cause friction and hinder smooth operation, while coating delamination exposes the underlying material to corrosion and wear. Additionally, chipping and pitting create uneven surfaces that affect precision and efficiency. A magnified view reveals metal sticking to the tool and small abrasive marks. After prolonged cutting, this stuck metal was removed and came off with the coating material, causing damage to the tool faces and exposing the substrate. This process of metal adhesion and subsequent dislodgement not only leads to pitting on the tool faces but also compromises the overall integrity of the tool, reducing its lifespan and effectiveness. It is crucial to regularly inspect and maintain the tool to prevent such damage and ensure optimal performance.

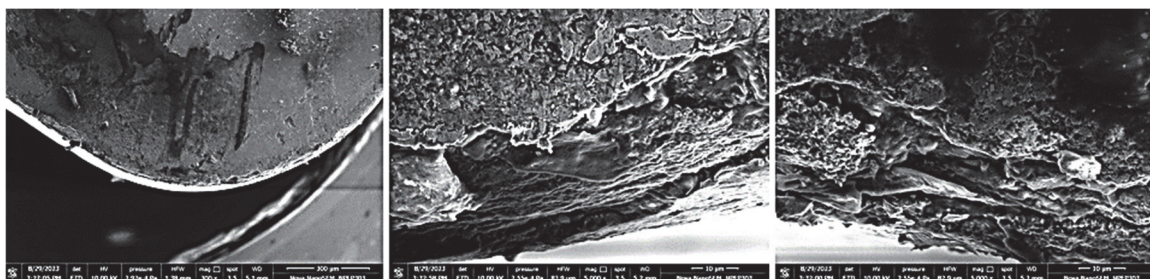


Figure 6: Tool images at run R1.

Hard particles from the tool flank surface, responsible for cutting, become trapped between the tool and machined surface during machining, causing them to rub against the tool flank. This rubbing action generates friction and heat, causing tool



wear and decreased machining efficiency. Additionally, the trapped particles can also result in surface defects or damage to the machined workpiece. Flank wear was discovered to be the predominant wear form.

Figs. 6–7 show coating abrasion by hard tool particles, which thereafter fracture owing to plucking of the attached material. This plucking phenomenon occurs due to the high stress and friction generated during the cutting process. The presence of hard tool particles further exacerbates the wear on the coating layers, leading to their eventual fracture. This type of wear is known as adhesive wear, where the hard particles from the tool flank adhere to the machined surface and cause friction. Due to this, the coating layers on the tool can become abraded and fractured. This indicates that at higher cutting speeds, adhesion becomes a significant factor in tool wear. The presence of adhesion suggests that the tool and workpiece materials are bonding together during the cutting process, leading to increased tool wear.

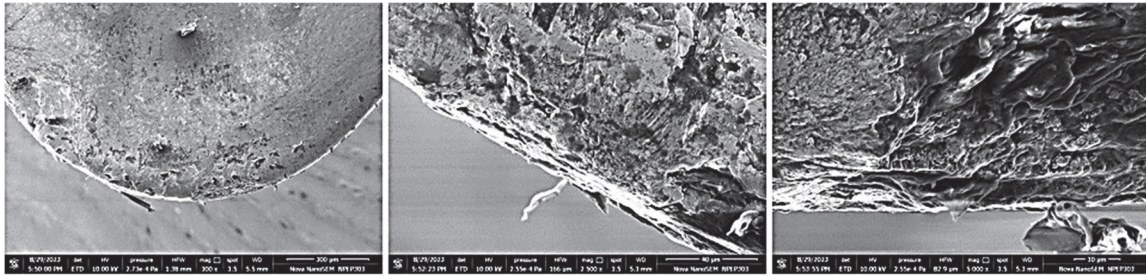


Figure 7: Tool images at run R5.

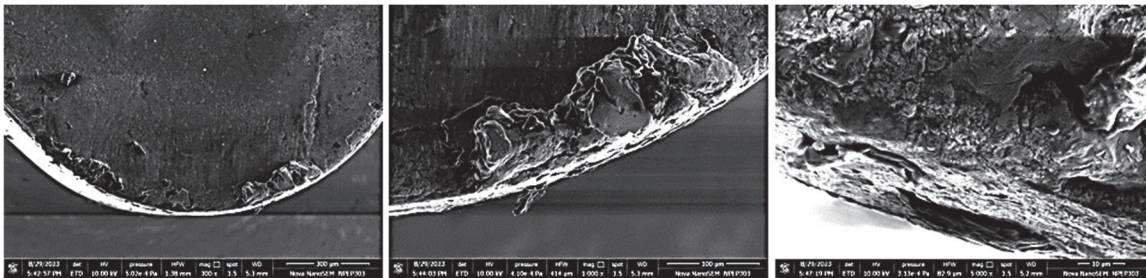


Figure 8: Tool images at run R9.

However, when turning at a lower cutting speed, pitting on the tool face with metal adhesion was found as a predominant wear mechanism. Figs. 8 depict the tool condition when turning a workpiece at run 9, as given in Tab. 2. In this figure, severe nose damage can be observed with metal adhesion and pitting. Fig. 9 shows fine abrasion marks and thinly adhered material on a tool that depicts the tool condition when turning at run 3, as given in Tab. 2. Fast-flowing chips cause tool material fragmentation due to the loss of adhering metal from the tool surface. Fig. 9 shows significant nose damage and pitting on the rake face, suggesting large tool wear. However, severe pitting and metal adhesion on the tool flank face, as shown in Fig. 10, reveal that adhesion as a predominant wear mechanism. The metal attached to the tool surfaces was removed at high sliding speed, resulting in the formation of shallow pockets, as depicted in Fig. 10 (run 10).

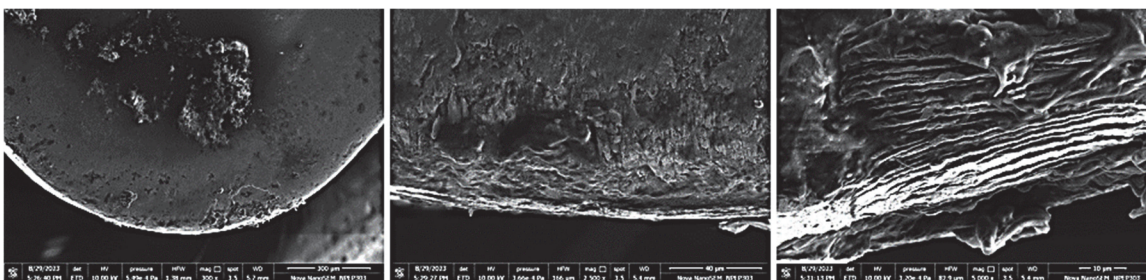


Figure 9: Tool images at run R3.

Immediately following the loss of the coating layer(s), especially while rotating at higher speeds, it was typical to see rapid degradation of the cutting edge that finally resulted in catastrophic failure. On the tool faces, the coating had completely peeled off, and the cutting edge had deformed plastically. The higher cutting speeds and significant compressive pressures

caused the cutting edge to distort plastically. The coating was removed due to the cracking of adherent metal on the tool surfaces. The outcome was the creation of a rough surface at the tool faces due to the fracture of tiny tool components that were taken away with the chips. Adhesion and pitting on the substrate were noticed as prime wear mechanisms. When the cutting was continued with a dull (fractured or severely damaged) cutting edge, it underwent plastic deformation because of the rise in loads and cutting temperature.

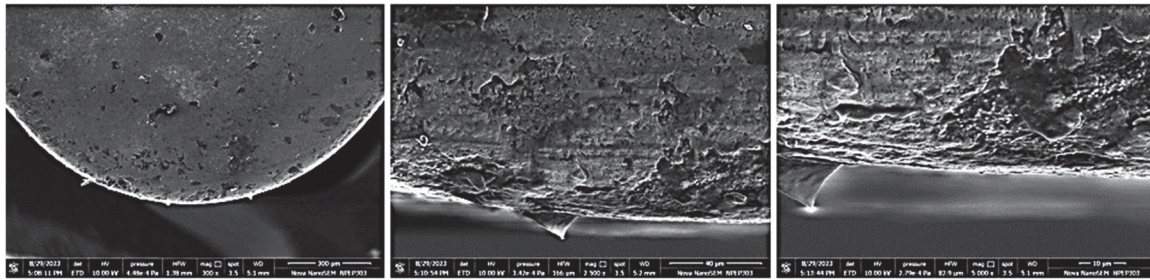


Figure 10: Tool images at run R10.

Empirical flank wear growth model

In order to estimate the flank wear, an experimental-based mathematical model is created, considering the machining time and the impact of the cutting parameters. A flank wear growth model is created using 214 observations of flank wear growth gathered under different cutting conditions (Figs. 3 and 4). Experimental flank wear observations were used to calibrate the models. DataFit software was used to find the unknown coefficients and exponents of a model by reducing the least square error between anticipated and experimental flank wear. Final flank wear growth equation is shown by Eqn. (1).

$$VB = 0.00109V^{0.7758} f^{0.4541} d^{0.2647} t^{0.7466} \tag{1}$$

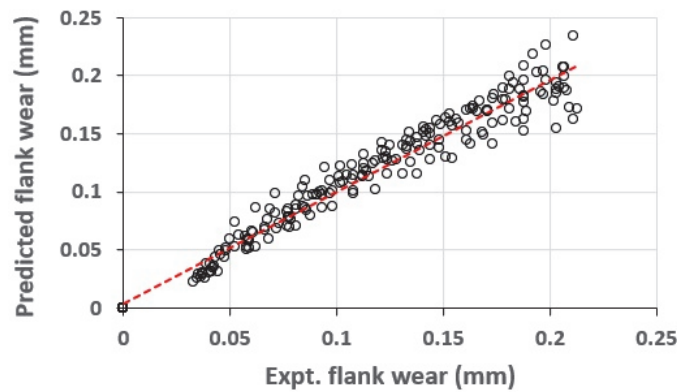


Figure 11: Anticipated and Experimental flank wear values when turning AISI 304 stainless steel.

The flank wear growth was predicted using Eqn. (1). Fig. 11 displays a plot of experimental and anticipated flank wear at several cutting conditions. Because the correlation coefficient achieved between the experimental and anticipated values was 0.935, the proposed equation may be utilized to analyze the flank wear growth for a specified tool-workpiece pairing in turning. All the points can be seen nearly falling on a line with a slope of 45°.

To properly comprehend the impact of a particular input parameter on flank wear, the established equations were simplified to a two-parameter level. This simplification allowed for a more efficient analysis of each input parameter on flank wear, leading to a clearer understanding of their influence. The computed flank wear values and the matching input parameter are presented on graphs. Figs. 12 illustrate how cutting parameters affect the development of flank wear for machining durations of 5 and 15 minutes.

The amount of tool wear is influenced by cutting time, cutting parameters, workpiece-tool combination, cooling methods, etc. It is frequently observed that tool wear rises as cutting parameters increase. The flank wear does indeed rise pronounceably with the cutting speed and cutting time, as seen in Fig. 12. This is supported by the fact that the exponent for cutting speed is greater than the other parameters, as seen in Eqn. (1). However, the exponent values do not differ much

for the cutting speed and machining time. The generation of higher cutting temperatures, which increase flank wear rate, may be the cause of the rise in flank wear with higher cutting speeds and cutting duration.

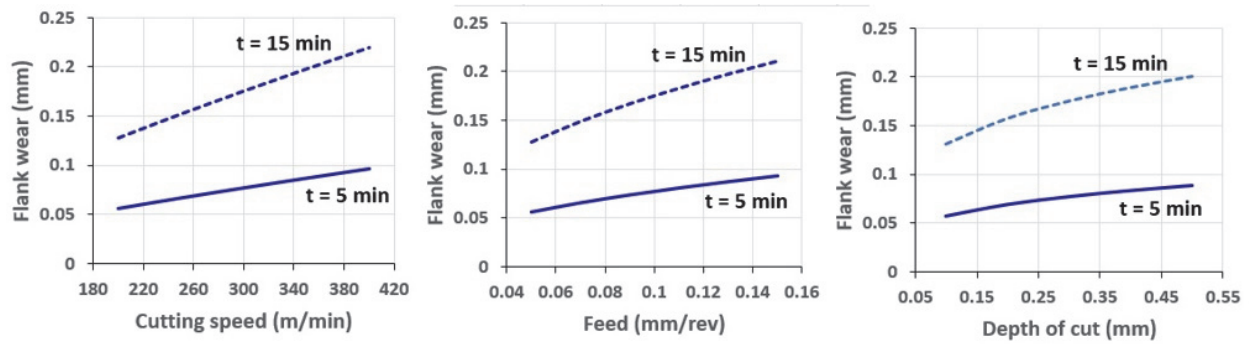


Figure 12: Flank wear at different machining times varying with cutting speed, feed, and depth of cut.

Artificial neural network (ANN) flank wear growth model

A computer method called an artificial neural network (ANN) can simulate connections between input parameters and output responses. Multilayer perceptron, or MLP, is the name of a fully linked multi-layer neural network. A typical feedforward artificial neural network is an MLP. The direction of information flow in feedforward propagation is forward. In the hidden layer, the input is utilized to create an intermediate function, which is subsequently used to generate an output. Fig. 13 is an example of a common MLP design that is in use. MLP is characterized by three different layers namely input layer, hidden layer, and output layer which consist of an interconnected group of artificial neurons. The number of neurons present in the input layer and output layer is equal to the number of input variables and corresponding output values.

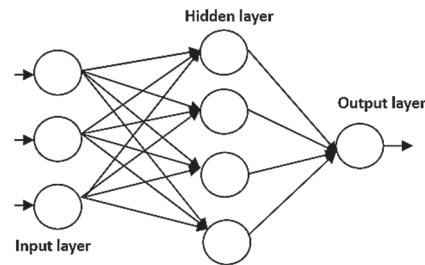


Figure 13: Typical ANN architecture.

The domain provides raw input to the input layer. At this layer, no calculation is done. Here, neurons only transmit data to the hidden layer. The neurons that make up the hidden layer are opaque to the outside world and offer the neural network abstraction. The characteristics entered through the input layer are subjected to various computations by the hidden layer, which then forwards the result to the output layer. The last layer of the network, known as the output layer, is responsible for bringing the knowledge gained from the hidden layer together and producing the desired outcome. Most of the time, all buried layers have the same activation function. However, the output layer's activation function typically varies from the hidden layer's activation function. The model's choice depends on its goal or type of prediction.

The network must be trained if output predictions are to be made with greater accuracy. An ordered modification of the network's synaptic weights occurs during a model's training phase in order to get the desired result. The error backpropagation method is the most often used training algorithm. The initialization of the weights and thresholds occurs in the first phase of a standard ANN algorithm. Following that, each neuron's output is computed based on its input data and initialization weights, which results in the network's final output prediction. The weights are then adjusted based on the output node error, which is determined next. Additionally, back-propagating faults computed at output layer nodes are used to alter the weights in the preceding layers [8]. The training ends when the ANN output is sufficiently close to the predicted output for each set, and this procedure is repeated for each pair of input and output training data.

Training of an ANN flank wear growth model

A neural network is a supervised machine learning algorithm to solve classification or regression problems with different sizes and depths. However, one need to preprocess input features, initialize the weights, add bias if needed, and choose

appropriate activation functions. Deciding on the architecture of a neural network is a big step in model building. During the training phase, the aim is to minimize the error rate as well as make sure that the model generalizes well to new data. A good model is one that does not overfit or underfit the data. A flow chart of the training of the ANN flank wear growth model is depicted in Fig. 14.

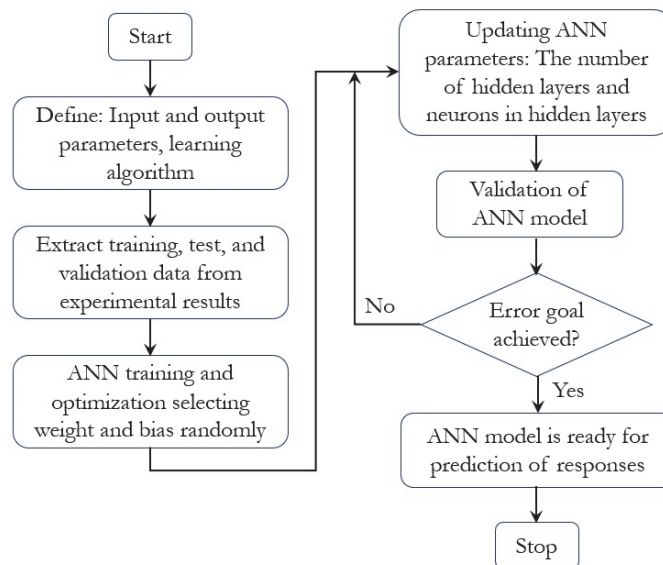


Figure 14: Flow chart of the training of the ANN flank wear growth model.

ANN models use parameters and hyperparameters, which are modified during training based on data. Parameters such as weights and biases are optimized during backpropagation to reduce costs. Hyperparameters are predetermined values that can be manually modified, but determining optimal values can be challenging due to dataset size and composition. Hyperparameters like hidden layers, neurons, activation function, learning rate, loss function, epochs, optimizer type, batch size, and others directly affect the structure and training process of an ANN. Hyperparameter values also have a major impact on prediction accuracy, algorithm execution time, and computational cost.

The larger and more complex the dataset, the more hidden layers a neural network requires to identify significant non-linear patterns in the data. This determines the neural network's learning capacity. A smaller network with fewer hidden layers may not fit the training set, unable to recognize intricate patterns or effectively predict unknown data. A bigger network that has too many hidden layers may overfit the training set. Rather than identifying patterns in the data, that kind of network attempts to memorize the training set. Consequently, the generalization of that kind of network to unknown data is poor. The number of hidden neurons (the number of neurons on hidden layers) in a network impacts its learning capacity. Too many neurons can create large networks that overfit training data, while too few can create smaller networks that underfit. Large neural networks require significant computational resources.

An activation function determines whether a neuron's input is important in predicting a network using mathematical operations. It derives output from input values, introducing non-linearity in hidden layers and using regression for one neuron in the output layer. The optimizer's task is to minimize the loss function by updating network parameters. Gradient descent is a popular optimization algorithm, requiring tiny steps to descend the error curve. The learning rate, a crucial hyperparameter in neural network training, determines the speed and direction of the step. It is best to start with a small learning rate like 0.001 and gradually increase it if necessary.

The loss function, which calculates the error between the anticipated and actual values, is used to assess a neural network's performance during training. The objective is to use an optimizer to minimize the loss function. Mean squared error (MSE), mean absolute error (MAE), or mean percentage error are the possible types of loss functions. Another significant hyperparameter is the epoch. The number of times the model views the complete dataset is referred to as an epoch. When the network is trained with a very modest learning rate or when the batch size is too small, the number of epochs should be raised. The network may occasionally tend to overfit the training set when using several epochs.

The study utilized MATLAB software for ANN training and prediction analysis, utilizing the neural network toolbox. Various ANN networks were built by varying the number of hidden layers and neurons in the hidden layers. The performance of ANN networks was assessed by plotting training and test errors against epochs. The number of epochs was set before training a neural network model, ensuring all data was used exactly once in one cycle. If the number of epochs is

chosen too low during the model-building phase, the training will end before the model converges. On the other hand, the data will be overfitted if the number of epochs chosen is very high. Furthermore, it is a waste of time and computational power. In the present study, the maximum number of epochs and the learning rate were set at default values of 0.01 and 1000, respectively. The error goal was set to zero. Computational time was not a constraint when developing an ANN model. It was set to infinite time. The ANN parameters and system configuration that were used in the construction and analysis are given in Tab. 3.

ANN parameter	Characteristics	System configuration
Number of hidden layer(s)	1, 3, and 5	An x64-based PC (LENEVO, Model: 81Y4) with a processor Intel(R) Core (TM) i7-10750H CPU @ 2.60GHz, 2592 MHz, 6 cores, and 12 logical processors
Number of neurons on hidden layer	10, 30, and 50	
Number of epochs (max)	1000	
Learning rate	0.001	
Rate of train data (random)	70%	
Rate of test data (random)	30%	
Learning algorithm	Levenberg-Marquardt backpropagation technique	
Transfer function	Tansig (tangent sigmoid)	
Learning rule	Back propagation	

Table 3: ANN model parameters and system configuration in the construction and analysis.

Using the MATLAB Toolbox, an ANN model is developed to obtain the flank wear growth varying with the cutting parameters and cutting time. Input, output, and hidden layers make up the three levels of the ANN design (Fig. 15). Four numbers of neurons (for input variables such as cutting speed, feed, depth of cut, and machining time) are present in the input layer; one is present in the output layer (for predicting flank wear growth), and the necessary number of neurons are present in the hidden layer(s). An array of numerical inputs is mapped to an array of numerical targets using a feed-forward neural network. The MATLAB Toolbox Neural Fitting program will assist in the selection of data, the design and training of a network, and the evaluation of its performance using regression analysis and mean squared error. Given reliable data and adequate hidden layer neurons, a two-layer feed-forward network with sigmoid hidden neurons and linear output neurons is arbitrarily chosen to suit multi-dimensional problems. The hyperbolic tangent sigmoid transfer function (tansig) given in Eqn. (2) was used as the transfer function.

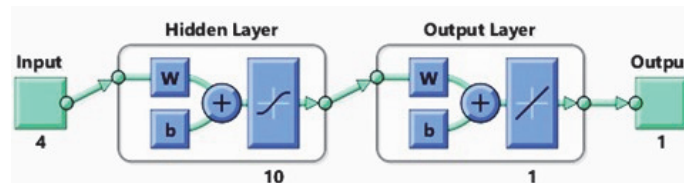


Figure 15: ANN architecture to obtain flank wear growth.

$$f(N) = \tanh(N) = \frac{2}{1 + e^{-2N}} - 1 \tag{2}$$

where $f(N)$ is the hyperbolic tangent sigmoid transfer function.

The Levenberg-Marquardt method, Bayesian regularization, and scaled conjugate gradient algorithms can be used to train the network. In this study, the Levenberg-Marquardt method has been primarily used because it is quicker than other algorithms. However, this approach nevertheless uses more memory. Three different types of samples are employed in neural networks for the training and validation of test data. Approximately 70% of the data is used to train the neural network. About 15% of the data is used to verify the predicted outcomes of the trained neural network. These validation data sets are employed to gauge network generalization and stop training when generalization reaches a certain point. Around 15% of the data is utilized for testing the predicted results by the neural network. These data sets do not influence training and provide an independent measure of network performance during and after training. The ANN model is developed by analyzing 170 flank wear observations under various cutting conditions and machining times, as shown in Tab. 4.



Expt. run	Cutting speed (V) (m/min)	Feed (f) (mm/rev)	Depth of cut (d) (mm)	Number of observations used for ANN		Observations can be referred from
				Training	Testing	
R1	300	0.1	0.5	15	3	Fig. 3
R2	350	0.08	0.4	10	2	Fig. 3
R3	350	0.12	0.4	9	2	Fig. 3
R4	250	0.08	0.4	10	2	Fig. 3
R5	250	0.12	0.4	10	4	Fig. 3
R6	300	0.05	0.3	6	4	Fig. 3
R7	300	0.1	0.3	13	3	Fig. 3
R8	300	0.15	0.3	14	5	Fig. 3
R9	200	0.1	0.3	9	3	Fig. 4
R10	400	0.1	0.3	7	3	Fig. 4
R11	350	0.08	0.2	11	3	Fig. 4
R12	250	0.12	0.2	14	3	Fig. 4
R13	350	0.12	0.2	16	2	Fig. 4
R14	250	0.08	0.2	12	2	Fig. 4
R15	300	0.1	0.1	14	3	Fig. 4

Table 4: Training and testing data set (flank wear observations) used for an ANN model.

The performance of the ANN model was evaluated by varying the number of hidden layers and neurons within them. Examining learning curve graphs is a typical practice for determining the convergence of neural network models. Typically, a graph of loss (or error) versus epoch is displayed. It is anticipated that as the number of training epochs rises, the accuracy will increase, and the loss will fall. After a while, they will, however, stabilize. After undergoing several training epochs, a neural network should eventually converge. Tab. 5 depicts the performance of ANN networks varying with the number of hidden layers and neurons within them. Mean squared error (MSE), computational time, and regression coefficient (R) values were used as performance criteria for the best model selection.

No. of hidden layers	No. of hidden neurons	Epoch	Learning rate	Computational time (seconds)	Mean squared error ($\times 10^{-5}$)	Regression coefficient (Overall)
1	10	1000	0.001	12	3.43	0.9975
1	30	1000	0.001	29	3.26	0.9986
1	50	1000	0.001	38	3.84	0.9979
3	10	1000	0.001	70.2	3.05	0.9983
3	30	1000	0.001	123	3.11	0.9983
3	50	1000	0.001	135.6	3.77	0.9976
5	10	1000	0.001	91.2	3.99	0.9967
5	30	1000	0.001	139.2	3.37	0.9961
5	50	1000	0.001	142.2	4.46	0.9951

Table 5: Performance of ANN networks.

From Tab. 5, the computational time (the time an ANN model took to converge) can be seen as increasing with the number of hidden layers and neurons within them. The lowest mean squared error and the highest regression coefficient (overall for the entire data set) can be obtained with one hidden layer and 30 neurons. The number of neurons can be seen as having a greater impact on ANN performance than hidden layers. It is found that the flank wear growth can be reliably predicted using an ANN model with one hidden layer and 10–30 neurons, considering a maximum number of epochs and the learning



rate of 0.01 and 1000, respectively. However, this study considered an ANN model using one hidden layer with ten neurons for further discussion, considering its lowest computational time and better prediction accuracy in comparison to other ANN models.

Fig. 16 depicts the training performance of an ANN model using one hidden layer with ten neurons. The optimal validation performance was achieved at epoch 139, with a score of 3.989×10^{-5} with a prediction accuracy of 0.9975. The average squared error between objectives and outputs, or mean squared error, is used to assess the effectiveness of neural network training. Lesser values are preferable. The correlation between outputs (predicted values) and goals (inputs) is measured by regression (R-squared) values. Figs. 17(a), (b), (c), and (d) illustrate neural network regression graphs with regression coefficients discovered during model training, validation, and testing, as well as for the complete data set. In the developed ANN model, regression coefficient values obtained can be seen as 0.9934 for training data, 0.9928 for test data, and 0.9936 for validation data.

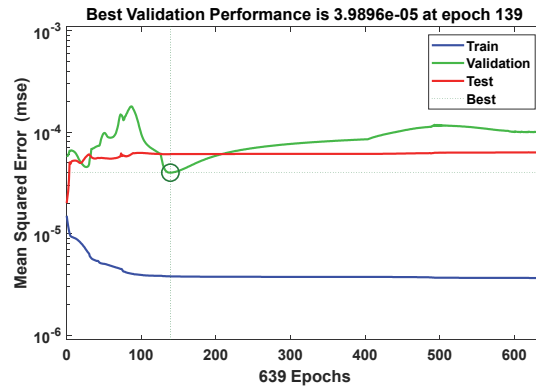


Figure 16: Neural network training performance.

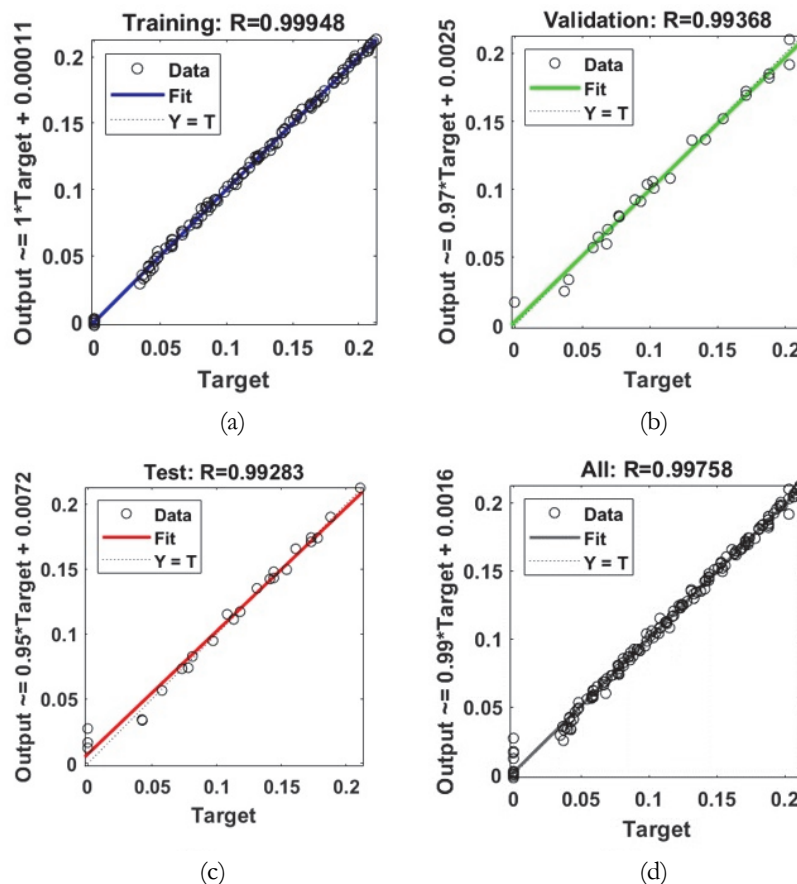


Figure 17: Neural network (a) Training, (b) Validation, (c) Test, (d) All data set.



Expt. run	Cutting speed (V) (m/min)	Feed (f) (mm/rev)	Depth of cut (d) (mm)	Time (min)	Flank wear (mm)		
					Experimental	ANN model	Empirical model
1	300	0.1	0.5	9.38	0.138	0.133	0.142
2	300	0.1	0.5	10.56	0.144	0.145	0.155
3	300	0.1	0.5	11.69	0.153	0.156	0.167
4	350	0.08	0.4	4.60	0.088	0.097	0.080
5	350	0.08	0.4	6.07	0.108	0.116	0.098
6	350	0.12	0.4	2.07	0.0618	0.066	0.053
7	350	0.12	0.4	3.07	0.081	0.082	0.071
8	250	0.08	0.4	4.35	0.0591	0.069	0.059
9	250	0.08	0.4	6.45	0.078	0.087	0.079
10	250	0.12	0.4	2.90	0.0578	0.055	0.052
11	250	0.12	0.4	4.30	0.0765	0.069	0.070
12	250	0.12	0.4	13.15	0.188	0.170	0.162
13	250	0.12	0.4	14.28	0.209	0.180	0.172
14	300	0.05	0.3	11.43	0.0843	0.066	0.105
15	300	0.05	0.3	14.16	0.102	0.073	0.123
16	300	0.05	0.3	16.84	0.125	0.082	0.140
17	300	0.05	0.3	19.47	0.141	0.115	0.156
18	300	0.1	0.3	15.93	0.174	0.175	0.184
19	300	0.1	0.3	17.10	0.183	0.187	0.194
20	300	0.1	0.3	18.24	0.194	0.200	0.203
21	300	0.15	0.3	6.49	0.101	0.098	0.113
22	300	0.15	0.3	7.35	0.113	0.109	0.124
23	300	0.15	0.3	8.19	0.123	0.120	0.135
24	300	0.15	0.3	11.40	0.164	0.163	0.172
25	300	0.15	0.3	12.16	0.173	0.173	0.181
26	200	0.1	0.3	12.63	0.112	0.112	0.113
27	200	0.1	0.3	14.60	0.135	0.131	0.126
28	200	0.1	0.3	16.54	0.148	0.152	0.138
29	400	0.1	0.3	6.31	0.124	0.134	0.115
30	400	0.1	0.3	7.30	0.144	0.155	0.128
31	400	0.1	0.3	8.27	0.163	0.177	0.141
32	350	0.08	0.2	6.18	0.077	0.077	0.083
33	350	0.08	0.2	7.67	0.091	0.093	0.097
34	350	0.08	0.2	9.16	0.107	0.107	0.111
35	250	0.12	0.2	7.16	0.081	0.085	0.086
36	250	0.12	0.2	8.54	0.0931	0.097	0.098
37	250	0.12	0.2	9.91	0.103	0.107	0.109
38	350	0.12	0.2	7.08	0.0851	0.085	0.110
39	350	0.12	0.2	8.04	0.0944	0.097	0.121
40	250	0.08	0.2	16.89	0.121	0.117	0.135
41	250	0.08	0.2	18.89	0.138	0.133	0.147
42	300	0.1	0.1	15.67	0.139	0.142	0.136
43	300	0.1	0.1	17.04	0.148	0.157	0.145
44	300	0.1	0.1	18.41	0.161	0.171	0.153

Table 6: Experimental and predicted flank wear values with ANN and empirical models.



Regression coefficients close to one for training, validation, and testing, and the entire data set demonstrates that the developed neural network model could be accurately applied to forecast flank wear growth of MTCVD-TiCN/Al₂O₃ coated tools when turning AISI 304 stainless steel. Further, the ANN model's accuracy is evaluated by predicting 44 flank wear observations at various cutting conditions and machining times (Figs. 3 and 4, Run 1 to 15). Tab. 6 displays the experimental and predicted flank wear values for different machining times and cutting conditions, excluding those used for model development. A comparison of the predicted results with the experimental-based mathematical model (empirical model) and artificial neural network (ANN) model is performed. The percentage error between the predicted and experimental wear growth for various process parameters is used to gauge the model's accuracy. Predicted results from ANN models can be seen to be in better agreement with the experimental values than empirical models. The average prediction error of 6.5% and 9.3% is observed for ANN and empirical models, respectively. It can also be confirmed from the experimental vs. predicted flank wear values using ANN and empirical models plotted at two different cutting conditions, as shown in Fig. 18. It is apparent that the results predicted by the ANN model are in better agreement with the experimental results as compared to the empirical model.

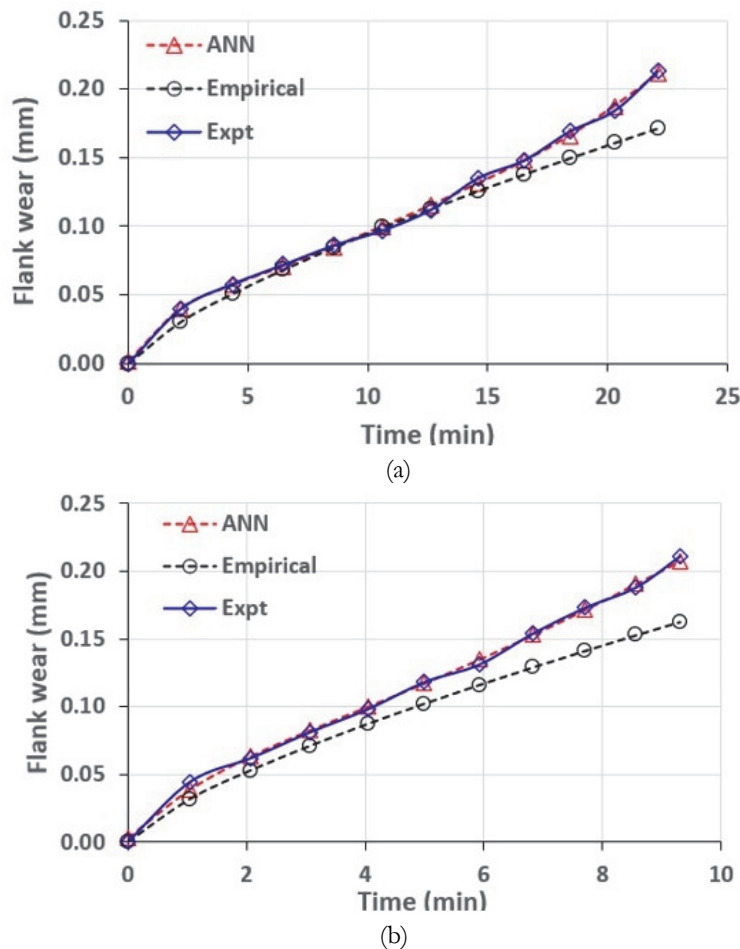


Figure 18: Experimental vs. predicted flank wear using empirical and ANN models at (a) Run 9 (b) Run3.

The experimental and projected flank wear values show good agreement. In the majority of cutting situations, tool failure happened because the coating layer broke off rather than the flank wear gradually wearing up to 0.2 mm. It can be confirmed from the tool wear SEM images, as shown in Figs. 4–10. The coating delamination, metal adhesion, pitting on the substrate, and cutting-edge chipping were seen for a specified tool-workpiece pairing in turning. As was previously mentioned, prolonged cutting causes metal adhesion and dislodgement, causing damage to tool faces, rake faces, and substrates, compromising tool integrity, lifespan, and effectiveness. The tool wear criterion of 0.2 mm is more realistic for achieving superior dimensional accuracy and surface quality while machining AISI 304 stainless steel using selected tools.



CONCLUSIONS

Flank wear, a gradual wear and tear on a tool's cutting edge during machining operations, is crucial for sustainable manufacturing. It affects product quality, and replacing tools before their tool life significantly impacts the machining economy. Accurate evaluation of flank wear allows manufacturers to replace tools at the optimal time, maximize tool life, and minimize production downtime. This proactive maintenance planning reduces the risk of sudden tool failure and potential workpiece damage. With this perspective, the study constructed ANN and empirical flank wear growth models while turning AISI 304 stainless steel with MTCVD-TiCN/Al₂O₃ coated carbide tools. The study provides several possible conclusions.

- The flank wear increased noticeably with the cutting speed and machining time. Empirical models developed also revealed that cutting speed, followed by machining time, was the most influential factor in flank wear.
- Adhesion and pitting on the substrate were observed as prime wear mechanisms. When cutting was continued while using a dull (fractured or severely damaged) cutting edge, it was found that the cutting edge underwent plastic deformation because of the rise in loads and cutting temperature.
- At higher cutting speeds, the tool failed because the coating layers peeled off due to the fast-moving chips breaking the attached metal, causing an abrupt fracture. Regular tool inspections could address potential issues before they cause abrupt fractures by identifying signs of wear or damage.
- In the developed ANN model, regression coefficient values obtained close to one for training, validation, and testing, and the entire data set demonstrates that the developed neural network model could be accurately applied to forecast flank wear growth of MTCVD-TiCN/Al₂O₃ coated tools when turning AISI 304 stainless steel.
- The predicted results by ANN models were in better agreement with the experimental values than the empirical model. The average prediction error of 6.5% and 9.3% was observed for ANN and empirical models, respectively.
- The tool wear criterion of 0.2 mm has been found to be more realistic for achieving superior dimensional accuracy and surface quality while machining AISI 304 stainless steel using selected tools, as prolonged cutting causes metal adhesion and dislodgement, causing damage to tool faces, rake faces, and substrate, compromising tool integrity, lifespan, and effectiveness.

REFERENCES

- [1] Singh, D. and Rao, P.V. (2010). Flank wear prediction of ceramic tools in hard turning. *Int. J. Adv. Manuf. Technol.*, 50, pp.479-493. DOI: 10.1007/s00170-010-2550-5.
- [2] Huang, Y. and Liang, S.Y. (2004). Modeling of CBN tool flank wear progression in finish hard turning. *ASME J. Manuf. Sci. Eng.*, 126(1), pp. 98-106. DOI: 10.1115/1.1644543.
- [3] Dawson, T.G. and Kurfess, T.R., 2006. Modeling the progression of flank wear on uncoated and ceramic-coated polycrystalline cubic boron nitride tools in hard turning. *ASME J. Manuf. Sci. Eng.*, 128(1), pp. 104-109. DOI: 10.1115/1.2039097.
- [4] Dureja, J.S., 2012. Optimisation of tool wear during hard turning of AISI-H11 steel using TiN coated CBN-L tool. *Int. J. Mach. Mach. Mater.*, 2, 12(1-2), pp.37-53. DOI: 10.1504/IJMMM.2012.048556.
- [5] Chinchanikar, S. and Choudhury, S.K., 2013. Modelling and evaluation of flank wear progression of coated carbide tools in turning hardened steels. *Int. J. Manuf. Technol. Manage.*, 27(1-3), pp.4-17. DOI: 10.1504/IJMTM.2013.058626.
- [6] Mohamad, A.K., Yusof, N.M., Ourdjini, A. and Venkatesh, V.C., 2008. The effectiveness of coatings when turning hardened cold work tool steel AISI D2 (60 HRC). *Int. J. Mach. Mach. Mater.*, 4(1), pp. 63-75. DOI: 10.1504/IJMMM.2008.020911.
- [7] Palanisamy, P. and Shanmugasundaram, S., 2008. Modelling of tool wear and surface roughness in hard turning using regression and artificial neural network. *Int. J. Mach. Mach. Mater.*, 4(1), pp.76-94. DOI: 10.1504/IJMMM.2008.020912.
- [8] Chinchanikar, S., Shinde, S., Gaikwad, V., Shaikh, A., Rondhe, M. and Naik, M., 2022. ANN modelling of surface roughness of FDM parts considering the effect of hidden layers, neurons, and process parameters. *Adv. Mater. Process. Technol.*, pp.1-11. DOI: 10.1080/2374068X.2022.2091085.
- [9] Savkovic, B., Kovac, P., Rodic, D., Strbac, B. and Klancnik, S., 2020. Comparison of artificial neural network, fuzzy logic and genetic algorithm for cutting temperature and surface roughness prediction during the face milling process. *Adv. Prod. Eng. Manage.*, 15(2), pp.137-150. DOI: 10.14743/apem2020.2.354.



- [10] Kulkarni, A., Sargade, V. and More, C., 2018. Machinability investigation of AISI 304 austenitic stainless steels using multilayer AlTiN/TiAlN coated carbide inserts. *Procedia Manuf.*, 20, pp.548-553. DOI: 10.1016/j.promfg.2018.02.082.
- [11] Sharma, N. and Gupta, K., 2019. Influence of coated and uncoated carbide tools on tool wear and surface quality during dry machining of stainless steel 304. *Mater. Res. Express*, 6(8), p.086585. DOI: 10.1088/2053-1591/ab1e59.
- [12] Chinchanikar, S. and Choudhury, S.K., 2014. Experimental investigations to optimise and compare the machining performance of different coated carbide inserts during turning hardened steel. *Proc. Inst. Mech. Eng., Part B: J. Eng. Manuf.*, 228(9), pp.1104-1117. DOI: 10.1177/0954405413500041.
- [13] Chinchanikar, S. and Choudhury, S.K., 2015. Predictive modeling for flank wear progression of coated carbide tool in turning hardened steel under practical machining conditions. *Int. J. Adv. Manuf. Technol.*, 76, pp.1185-1201. DOI: 10.1007/s00170-014-6285-6.
- [14] Singh, T., Dureja, J.S., Dogra, M. and Bhatti, M.S., 2018. Multi-response optimization in environment friendly turning of AISI 304 austenitic stainless steel. *Multidiscip. Model. Mater. Struct.*, 15(3), pp.538-558. DOI: 10.1108/MMMS-07-2018-0139.
- [15] Bedi, S.S., Sahoo, S.P., Vikas, B. and Datta, S., 2021. Influence of cutting speed on dry machinability of AISI 304 stainless steel. *Mater. Today Proc.*, 38, pp.2174-2180. DOI: 10.1016/j.matpr.2020.05.554.
- [16] Özbek, N.A., Karadag, M.I. and Özbek, O., 2020. Optimization of flank wear and surface roughness during turning of AISI 304 stainless steel using the Taguchi method. *Mater. Test.*, 62(9), pp.957-961. DOI: 10.3139/120.111571.